J. Appl. Comput. Mech., 6(3) (2020) 543-553
DOI: 10.22055/JACM.2019.29216.1573

ISSN: 2383-4536
jacm.scu.ac.ir

M&MoCS
Shahid Chamran University of Ahvaz

Journal of Applied and Computational Mechanics

Research Paper

Sealing Performance of the End Fitting of a Marine Unbonded Flexible Pipe under Pressure Penetration

Liping Tang[1], Wei He[1], Xiaohua Zhu[1], Yunlai Zhou[2]

[1] School of Mechatronic Engineering, Southwest Petroleum University
Chengdu, 610500, China, Email(s): lipingtang@swpu.edu.cn, hewei@stu.swpu.edu.cn, zhuxh@swpu.edu.cn

[2] Department of Civil and Environmental Engineering, National University of Singapore
Singapore, 117576, Singapore, Email: YunLai.zhou@alumnos.upm.es

Received April 20 2019; Revised June 12 2019; Accepted for publication July 02 2019.
Corresponding authors: Liping Tang (lipingtang@swpu.edu.cn), Xiaohua Zhu (zhuxh@swpu.edu.cn)

Abstract. The sealing performance of end fittings is very important for offshore oil and gas pipelines. To investigate the sealing behavior of a ring-shaped wedge seal, global and local numerical models of the ring–pipe interaction have been developed based on the finite-element method. First, the sealing process of the ring under pressure is simulated. Second, a criterion for the penetration of fluid pressure is applied in these models to assess how the sealing capacity changes along the contact surface. Finally, the contact magnitude of interference and the shape of the sawtooth heaves on the sealing ring are predicted and compared. The results show an interesting concentration of von Mises stress in the sealing ring and also that the peak contact pressure appears in the sealing zone. However, the penetration of fluid pressure has obvious effects on the distributions of von Mises stress and contact pressure. The best sealing performance is when the axial displacement of the sealing ring is 1.4 mm and the contact magnitude of interference is 0.3 mm. Given the sawtooth heave of sealing ring, semicircular heave gives the better sealing capacity compared with trapezoidal heave.

Keywords: Marine unbonded flexible pipe; Sealing performance; Finite-element method; Pressure penetration; Contact pressure.

1. Introduction

Oil and gas resources are the main driving forces for social development and progress and are expected to increase to meet the future requirements for power and heat. As the main energy sources for modern society, they occupy an extremely important strategic position [1]. As onshore and shallow-water oil reserves become depleted, so the oil industry turns to less-accessible locations [2]. Compared with onshore oil reserves, offshore oil and gas resources are particularly rich. However, the exploitation environment is so harsh that the requirements for oil and gas equipment are higher [3, 4]. The necessity to exploit offshore oil and gas fields has motivated the development of new pipe technologies and extended the application of pipe [5]. One type of pipe is the unbonded flexible pipe that is used for production, injection, and gas lift lines because of its ability to bear harsh environmental loads and adapt to the movements of floating production units [6]. Because of their technical and economic advantages, unbonded flexible pipes are replacing rigid pipelines and becoming the dominant transportation equipment for offshore oil and gas [7].

An unbonded flexible pipe usually comprises several concentric layers that provide the flow line with its flexibility and strength. It may be used to couple a rigid flow line or another flexible flow line to a floating vessel to convey oil and gas

Published online: September 20 2019

for transport. An end fitting can be used to couple the flexible pipe at each end to a flow line or wellhead. In the marine flexible pipeline system, the end fitting (as shown in Fig. 1) is an essential component with the function of connecting the pipes, the floating production storage and offloading, and the underwater production facilities [9]. If the sealing performance fails under functional and environmental loads, then an oil and gas leakage accident may occur and result in serious consequences. Therefore, analyzing the sealing performance of the end fitting of an unbonded flexible pipe is a necessary step during the design and manufacture process.

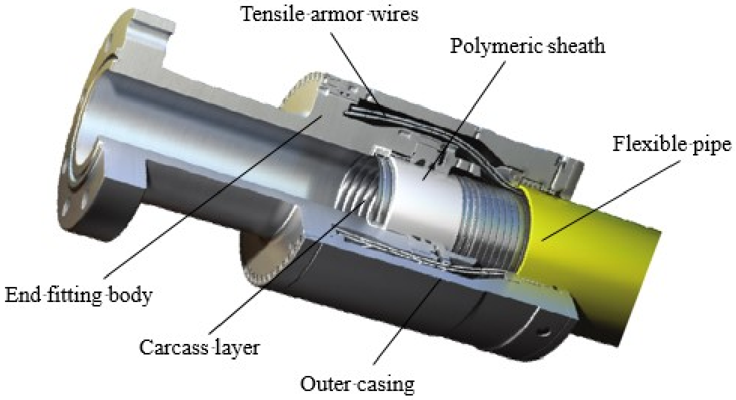

Fig. 1. Typical cross section of flexible-pipeline end fitting [8].

In fact, there has been much research on such sealing structures in recent years. Hu et al. [10] established a two-dimensional axisymmetric model of the inserted sealing ring and considered how various system parameters and operating conditions influence the sealing performance; they concluded that the concentration of stress at the shoulder and the inner vertex of the sealing ring directly affects the life of the sealing ring, and they proposed a new design with optimized geometric parameters. Zhou et al. [11] and Wu et al. [12] studied the sealing performance of O and wedge rings, respectively, which are commonly used in engineering. The former used numerical finite-element (FE) simulation, while the latter was more theoretically inclined and proposed a novel stress-distribution analytical model.

As for research on the sealing structure of pipeline end fittings, Wang et al. [13] investigated the effect of critical condition on the performance of the sealing structure and created a new method for analyzing the contact pressure of the sealing surface by analyzing the static metal seal mechanism; they also proposed an optimized design for a new subsea pipeline mechanical connector. Fernando et al. [14, 15] developed an FE model of a flexible-pipe end-fitting sealing ring to evaluate the contact stress and compared the contact pressure predicted by the FE method with actual contact-pressure measurements; they used an ultrasonic technique, thereby giving their work significant promise. Li et al. [16] considered the sealing performance of a deep-water flexible-pipe end-fitting sealing system and established an FE model by using the ABAQUS software; they studied the key parameters under different conditions, and their results provided further references for research into flexible-pipe end fittings. By summarizing the general sealing criteria, Zhang [17] introduced the concept of the "contact-pressure amplification factor" to evaluate the sealing capability of an end fitting.

In previous studies, the end-fitting sealing criteria were analyzed and the geometric parameters of the sealing system were investigated and optimized. Different from those studies, the present one establishes a global and a local numerical model of the sealing-ring–pipe interaction respectively by FE means in ABAQUS. With these two models, the present study is focused on (i) the sensitivity of the contact magnitude of interference to the sealing capacity and (ii) how the pressure penetration influences the contact-stress distribution.

2. Structure of Flexible-pipe Ending Fitting

As the main equipment of the offshore oil and gas industry, the manufacture and application of marine unbonded flexible pipeline systems are subject to a unified standard [18, 19]. According to API SPEC 17J, the typical structure of a flanged flexible-pipe end fitting is shown schematically in Fig. 2, and Fig. 3 shows a simplified cross section of the sealing system. The outer casing (10) is connected to the end-fitting body (1) by using threads or bolts so as to protect the components in the end fitting. The wedge inner sealing ring (4) is the primary sealing component of the system and is pressed by the end-fitting body to produce sufficient sealing capacity. The sealing ring squeezes the polymeric sheath (5) against the inner carcass (8) of the flexible pipe. The inner sleeve (2), which is close to the carcass end ring (3) used to terminate the inner carcass, ensures the electrical insulation of the inner carcass. The inner sealing ring is activated by the inner flange (6) that is connected to the pressure armor (9). The outer sealing ring (11) is activated by the outer flange (12) that is connected to the outer casing. The tensile armor wires (7) are anchored by filling the internal voids of the end fitting with epoxy resin.

In traditional analysis, the sealing ring is usually simplified to shape A shown in Fig. 4, ignoring the sawtooth. However, in practical engineering the sealing ring is manufactured as either shape B (i.e., a semicircular sawtooth) or shape C (i.e., a trapezoidal sawtooth), and their performances are compared and discussed herein.

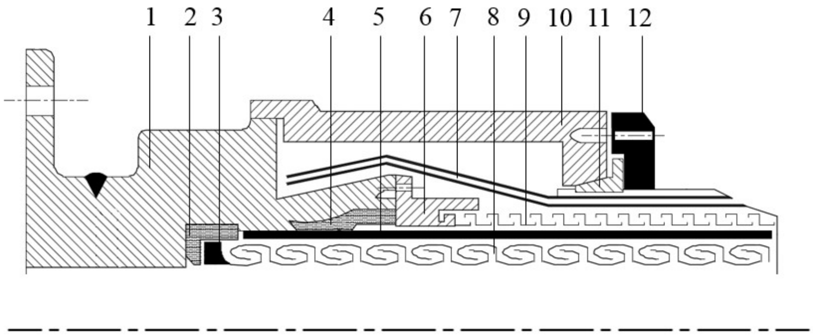

Fig. 2. Typical flanged flexible-pipe end fitting.
1: end-fitting body; 2: inner sleeve; 3: carcass end ring; 4: inner seal ring; 5: polymeric sheath; 6: inner flange; 7: tensile armor wires; 8: inner carcass; 9: pressure armor; 10: outer casing; 11: outer sealing ring; 12: outer flange

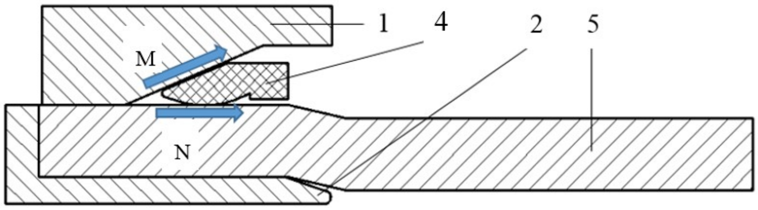

Fig. 3. Cross section of seal system.
1: end-fitting body; 2: inner sleeve; 4: inner sealing ring; 5: polymeric sheath

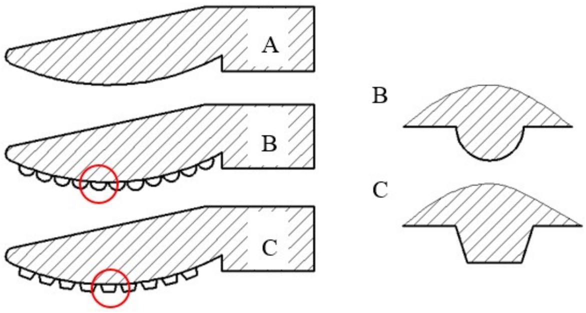

Fig. 4. Inner sealing ring with different sawtooth heaves

When the fluid acts on the inner sealing ring from the microscopic gap between the end-fitting body and the polymeric sheath of the flexible pipe, two leak paths M and N are created (as shown in Fig. 3). Path M refers to the metal-to-metal contact between the sealing ring and the end-fitting body. Because the contact path of this section is long and the metal contact stress is higher, and because it's sealing capacity is also related to the material's performance, this path is not the focus herein. Path N refers to the metal-to-polymer interfacial contact between the sealing ring and the polymeric sheath of the flexible pipe. This path involves complex interactions such as elastic-plastic deformation and nonlinear contact, and the contact pressure is lower in this path; it is therefore the main leak path and also the focus herein [13].

Seals can be divided into two categories, namely dynamic ones and static ones. The contact seal of the present sealing ring is a static one, the other two types of static seal being sealant and direct contact [20]. The sealing performance of this type of seal is evaluated by the amount of fluid leakage [14]. To achieve a lower rate of leakage and thus a higher sealing capacity, it is necessary to achieve a greater contact pressure, and the contact surface should be as long as possible to increase the resistance in the leak path. Increasing the contact magnitude of interference can raise these two indexes to a certain extent, but too high a magnitude of interference will destroy the performance of the sealing material itself. It is therefore necessary to estimate the magnitude of interference of the contact surface according to the actual situation.

3. Model of End-fitting Seal System

3.1. Finite-element model

In this section, a global and a local FE model of a flexible-pipeline end-fitting sealing system with a bore diameter of 139.7 mm and a design pressure of 20 MPa are developed. According to API SPEC 17J, the factory acceptance test pressure is 1.5 times the design pressure, meaning that the critical pressure acting on the end fitting is 30 MPa in service. A two-dimensional planar axisymmetric solid model is selected because of its axisymmetric geometry and load characteristics. The basic physical properties of each part are given in Table 1.

Table 1. Materials and properties for each part of the model.

Part	Young's modulus [GPa]	Poisson's ratio	Yield strength [MPa]
End-fitting body	210	0.3	355
Inner sleeve	210	0.3	355
Inner sealing ring	191	0.3	758
Polymeric sheath	0.571	0.45	20.74

It should be noted that the polymeric sheath of the flexible pipe is usually extruded from high-molecular-weight polymer materials such as high-density polyethylene [21]. Herein, the data for the polymeric material parameters are taken from Ref. 22, and the curve of the elastic-plastic properties of the polymeric material is shown in Fig. 5.

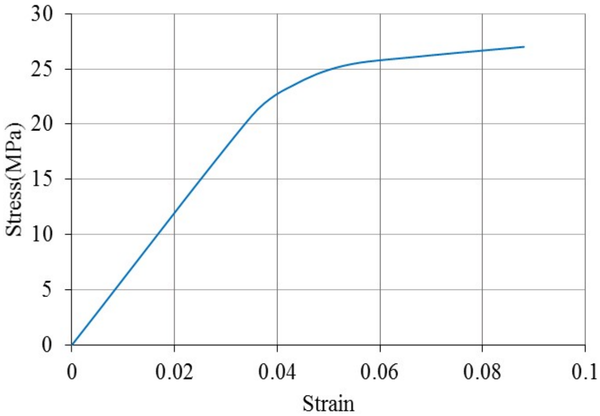

Fig. 5. Stress-versus-strain curve for the polymeric material.

With the nonlinear contact between the metal and the considered polymer ~~taken into account~~, the Mohr–Coulomb friction criterion is used to describe the contact relationship (i.e., normal contact is "hard" contact, and tangential contact involves setting the penalty function to 0.1) [15, 22, 23]. Given that the materials are either incompressible or quasi-incompressible, the planar axisymmetric hybrid element CAX4H is selected for these models. Structured and sweep meshing techniques are used in each part, and the mesh of the contact area is refined to improve the accuracy.

As for the boundary conditions and loads, the end-fitting body, the inner sleeve, and the polymeric sheath are completely fixed while the sealing ring is free. In the first step, the ring's sealing process is simulated by controlling load displacement An axial displacement is applied to the inner sealing ring in the global model, while a normal displacement is applied directly to a single sawtooth in the local model. In the second step, a pressure penetration of 30 MPa is applied in the two models along the arrow shown in Fig. 6, and the pressure penetration criterion is introduced in detail in Section 3.2. The FE models are shown in full in Fig. 6.

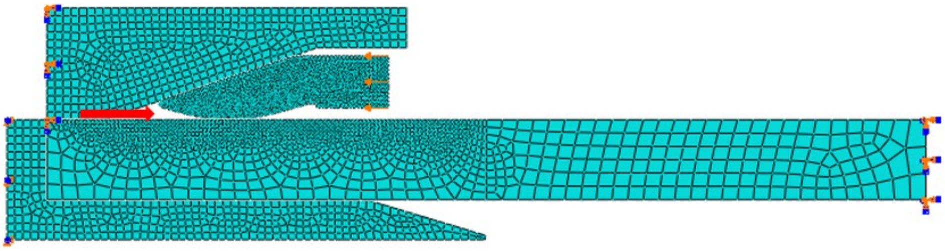

(a) Global model

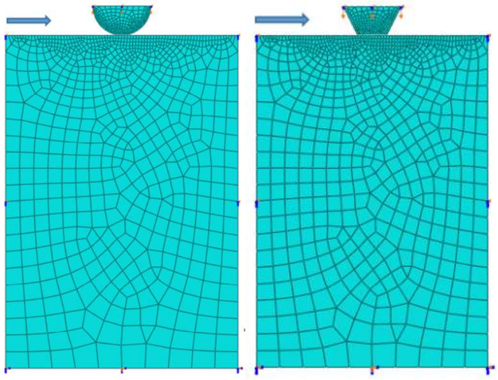

(b) Local model of a single sawtooth

Fig. 6. Global and local finite-element (FE) models.

3.2. Pressure penetration criterion

As mentioned above, in the second step of the local model, the pressure penetration criterion in the FE software is applied to the contact surface, and its principle is shown in Fig. 7 [24, 25]. The contact face with elements 3 and 4 is defined as the master surface, and the other surface with elements 1 and 2 is defined as the slave surface. Nodes 11 and 12 are on one side of the contact surface of element 1. As shown in the arrow direction of the Fig. 7, when the fluid penetrates from left to right, so the fluid pressure will load from left to right along the two surfaces. Node 11 is the first node that is exposed to the fluid pressure, and if the contact pressure on node 11 exceeds the applied fluid pressure, then the fluid will stop penetrating, making node 11 the critical point. If the contact stress is less than the fluid pressure, then the fluid will penetrate node 11 and continue flowing until a new node becomes critical by having the contact pressure exceed the fluid pressure. The pressure penetration criterion is akin to subjecting the contact surface to the actual fluid pressure, thereby simulating the actual effect of the fluid pressure on the performance of inner sealing ring and improving the accuracy to which the performance of the contact seal is evaluated [26, 27]. In fact, the characteristics of the pressure fluid are widely studied; for example, Liao et al. [28] investigated the permeability of cartilage contact gaps of different heights by developing a micro-scale computational fluid dynamics model.

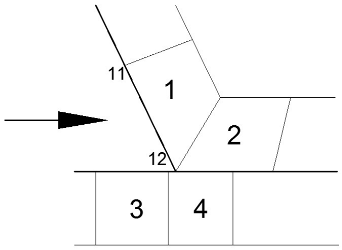

Fig. 7. Pressure penetration criterion for contact surface.

If fluid of pressure magnitude f has penetrated up to node 12 on the slave surface, then the variation of the distributed load over element 1 is given by:

$$P_1 = f\,N_1 + f\,N_2 = f \tag{1}$$

and the variation of the distributed load over element 2 is given by:

$$P_2 = f\,N_1 \tag{2}$$

where N_1 and N_2 are the shape functions on the face of a first-order element [29].

4. Results and Discussion

4.1. Sensitivity analysis of axial displacement of sealing ring

In the global end-fitting model, the magnitude of the interference between the sealing ring and the polymeric sheath of the flexible pipe is controlled by the axial displacement of the wedge inner sealing ring. To assess the influence of the magnitude of interference on the contact stress along the contact surface path N, different axial displacements (0.8, 1.0, 1.2, and 1.4 mm) are applied on the inner sealing ring according to the actual geometrical properties. How the sealing performance changes after pressure penetration is also analyzed, and these results are shown in Figs. 8 and 9.

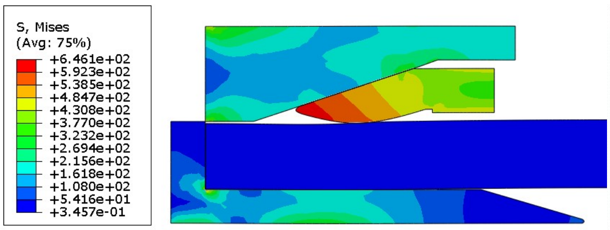

(a) Axial displacement: 0.8 mm

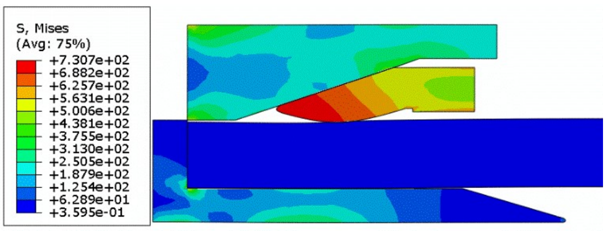

(b) Axial displacement: 1.0 mm

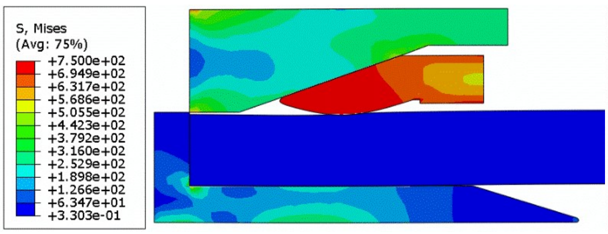

(c) Axial displacement: 1.2 mm

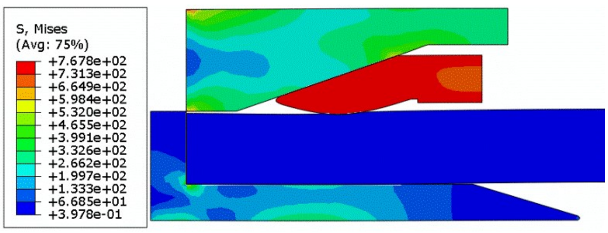

(d) Axial displacement: 1.4 mm

Fig. 8. von Mises stress distribution obtained from FE model.

The stress distribution in Fig. 8 shows that the main von Mises stress in the model is distributed on the sealing ring during the sealing process, and that the stress closer to the contact zone is higher while the stress of the end-fitting body and inner sleeve is lower. When the axial displacement of the sealing ring grows, the von Mises stress distribution changes slightly, but the maximum von Mises stress increases obviously from 646.1 MPa to 767.8 MPa with an increase of 19%. When the axial displacement is 1.4 mm (as shown in Fig. 8d), the maximum von Mises stress of the sealing ring exceeds the yield strength of 758 MPa, whereupon plastic deformation begins.

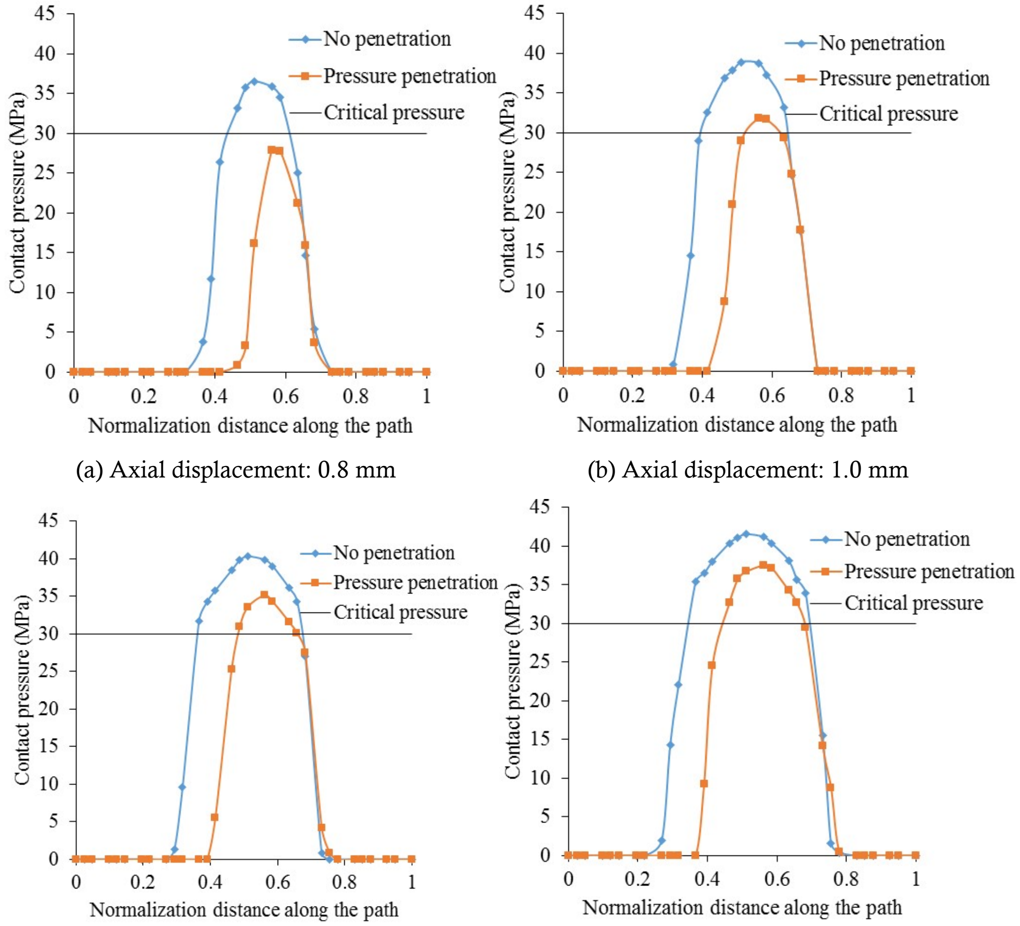

(a) Axial displacement: 0.8 mm (b) Axial displacement: 1.0 mm

(c) Axial displacement: 1.2 mm (d) Axial displacement: 1.4 mm

Fig. 9. Changes of contact pressure before and after pressure penetration.

As shown in Fig. 9, for each axial displacement, the peak contact pressure and its distribution along the contact surface path change significantly after pressure penetration. The contact pressure distribution is smooth and approximately axisymmetric when there is no pressure penetration. However, once pressure penetration is applied, the contact pressure distribution transfers to the right-hand side of the contact path (i.e., along the direction of pressure penetration). At this moment, the contact pressure becomes zero on the left-hand side, which means that the contact surfaces on left-hand side separate from each other because of the pressure and no longer create a seal.

In all four cases, the contact pressure drops after pressure penetration but the peak contact pressure remains above the critical fluid pressure, meaning that the sealing system continues to operate. In addition, Table 2 shows that the decrease ratio of contact pressure drops from 0.24 to 0.09 as the axial displacement increases from 0.8 mm to 1.4 mm, while the contact pressure increases gradually. With no pressure penetration, the peak contact pressure grows from 36.5 MPa to 41.5 MPa (i.e., by a factor of 0.13), and the length along the path also increases. With pressure penetration, the peak contact stress increases from zero to 37.5 MPa, and the contact surface changes similar to the contact stress.

In summary, when the axial displacement is insufficient, the sealing ring lacks sealing capacity, and when the axial displacement is large (1.4 mm), the seal ring begins to yield, thereby possibly accelerating its fatigue damage. Therefore, for the present end-fitting model, the sealing ring has the best sealing performance when the axial displacement is 1.2 mm.

Table 2. Variation of contact stress and maximum von Mises stress for different displacements.

Axial displacement		0.8 mm	1.0 mm	1.2 mm	1.4 mm
Contact pressure [MPa]	Before penetration	36.5	38.9	40.3	41.5
	After penetration	27.8	31.8	35.1	37.5
	Decrease ratio	0.24	0.18	0.12	0.09
Maximum von Mises stress of sealing ring [MPa]		646.1	730.7	750.0	767.8

4.2. Analysis of serrated shape of contact surface

The sawtooth structure of the sealing ring may affect the sealing performance. In this section, the sawtooth shapes of the three sealing rings shown in Fig. 4 are compared when the axial displacement of the sealing ring is 1.2 mm from the Section 4.1. The results show that using a sawtooth could increase the contact pressure along the leak path N (Fig. 10). As shown in Fig. 11, the three types of sealing ring change similarly after pressure penetration: each exhibits a decreased peak contact pressure and a transformed pressure distribution along the path. However, the seal contact pressure and the contact length are obviously greater for the semicircular and trapezoidal sawtooths compared to the case of no sawtooth. This is because a sawtooth has smaller contact area, making it easier for the sealing ring to be pressed into the polymeric sheath and thereby achieving greater contact pressure. However, the difference between the semicircular and trapezoidal sawtooths is not obvious, so more-detailed analysis is carried out in Section 4.3.

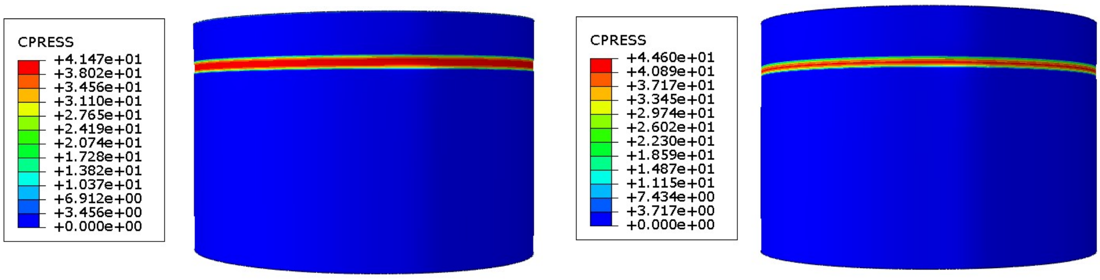

(a) No sawtooth (b) Semicircular sawtooth

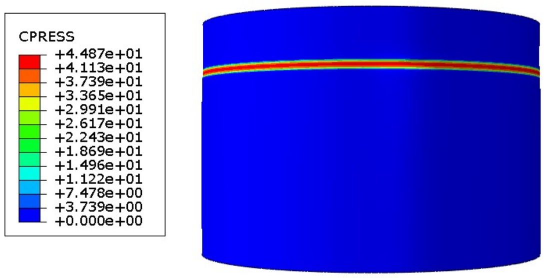

(c) Trapezoidal sawtooth

Fig. 10. Contact pressure distribution on polymeric sheath before pressure penetration.

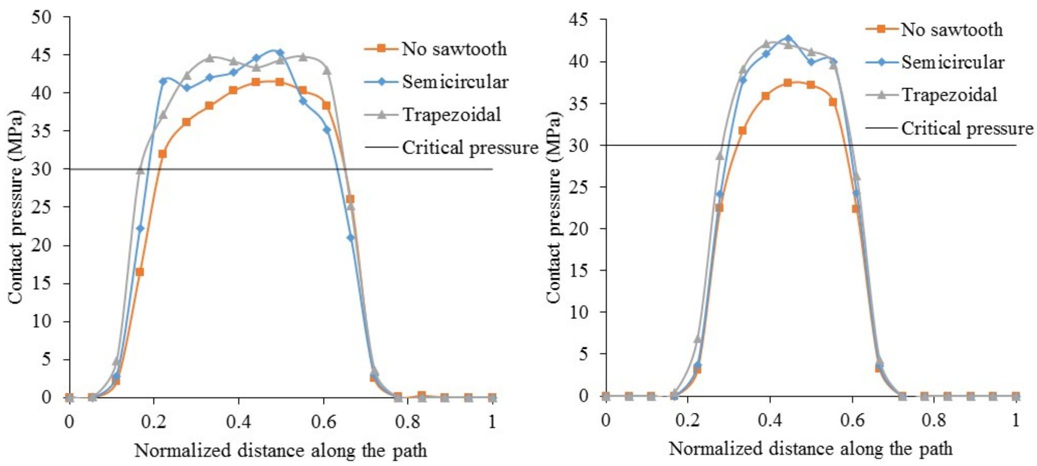

(a) Before pressure penetration (b) After pressure penetration

Fig. 11. Comparison of contact pressure for different serrated shapes.

4.3. Optimized analysis of single sawtooth

To compare further the performance of contact seals with semicircular and trapezoidal sawtooths, a local model of a single sawtooth of the sealing ring is established. How the contact pressure distribution varies with the magnitude of interference is shown in Fig. 12, and how the maximum contact pressure varies after pressure penetration is shown in Fig. 13. The distribution of contact pressure differs for the two sawtooth shapes. Furthermore, the maximum contact pressure of each sawtooth type increases with the interference, but the pressure distribution is almost unchanged. In addition, introducing the pressure penetration reduces the maximum contact pressure of the contact surface. Herein, the sealing ring has the best sealing performance when the contact magnitude of interference is 0.3 mm, so this case is discussed in detail.

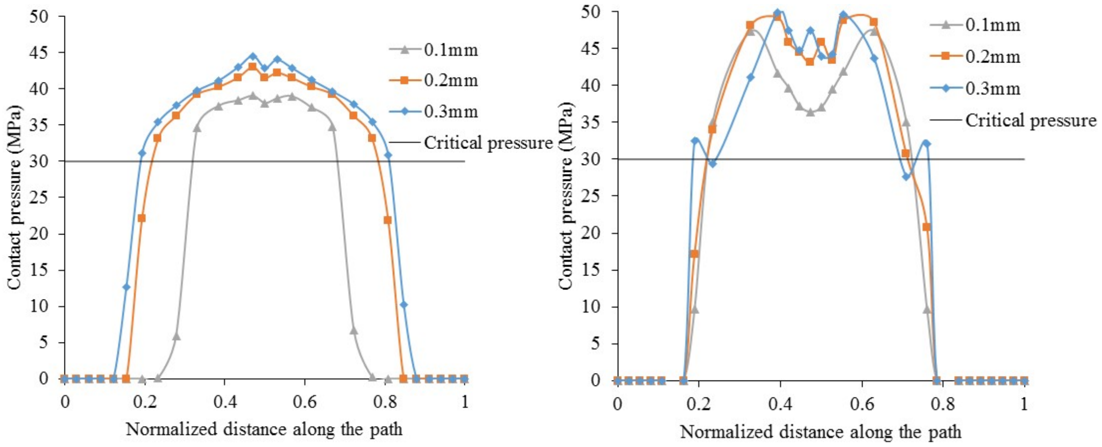

(a) Semicircular sawtooth (b) Trapezoidal sawtooth

Fig. 12. Distribution of contact pressure under different interference levels.

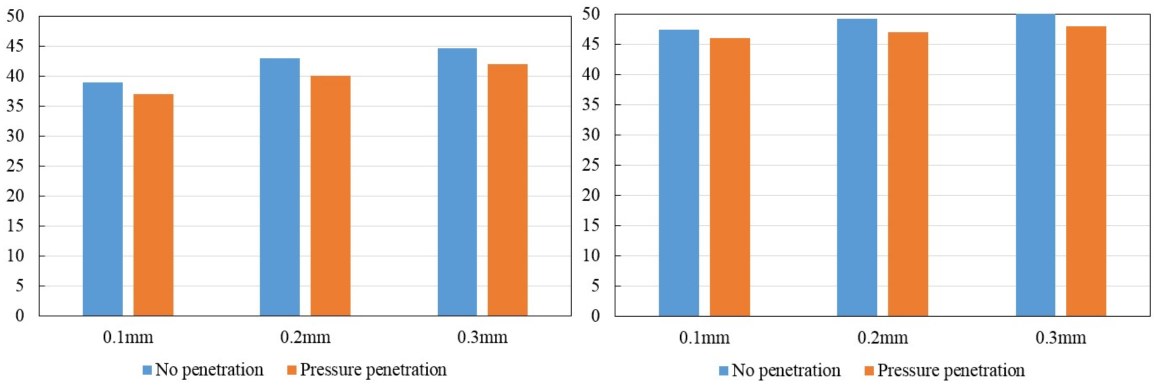

(a) Semicircular sawtooth (b) Trapezoidal sawtooth

Fig. 13. Variation of peak contact pressure after pressure penetration.

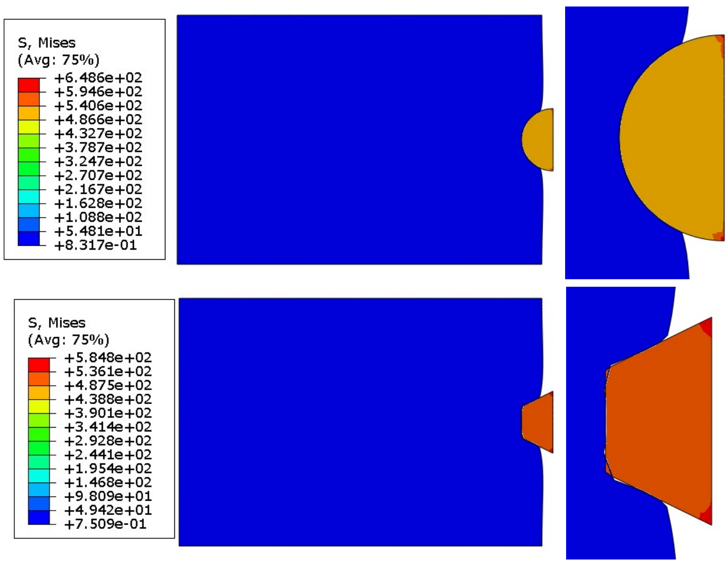

(a) Before pressure penetration

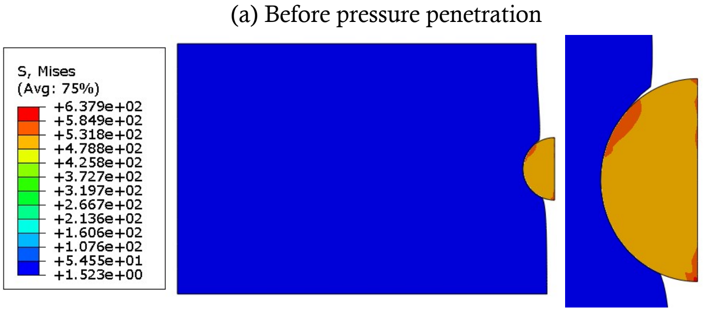

Fig. 14. von Mises stress distributions for different sawtooth shapes.

(b) After pressure penetration

Fig. 14. Continued.

Figure 14 shows the von Mises stress state of the two sawtooth shapes when the magnitude of interference is 0.3 mm. Before pressure penetration (as shown in Fig. 14a), the stress distribution is axisymmetric because of the symmetry of the geometry, boundary conditions, and loads of the model, and the von Mises stress is concentrated mainly on the sawtooth of the seal model. After pressure penetration (as shown in Fig. 14b), the stress distribution is no longer axisymmetric but has undergone a significant deflection, and the polymeric sheath is tilted toward the direction of fluid flos. Furthermore, there is a gap between the two contact surfaces because of the infiltration of pressure fluid.

The graph in Fig. 15 shows how the contact pressure varies after pressure penetration. With no pressure penetration, the maximum contact pressures of the semicircular and trapezoidal sawtooths are 45.6 MPa and 49.6 MPa, respectively. However, the contact pressure of the semicircular sawtooth is distributed smoothly, evenly, and approximately axisymmetrically, whereas that of the trapezoidal sawtooth fluctuates greatly and exhibits multiple peaks and troughs.

After pressure penetration, the respective maximum contact pressures decrease to 38.0 MPa and 47.3 MPa by factors of 0.16 and 0.04, respectively, compared with before penetration. The contact pressure distribution now deviates to the right-hand side, but that of the semicircular sawtooth still shows greater stability. Therefore, the sealing performance of the trapezoidal sawtooth is predicted to be poorer than that of the semicircular sawtooth.

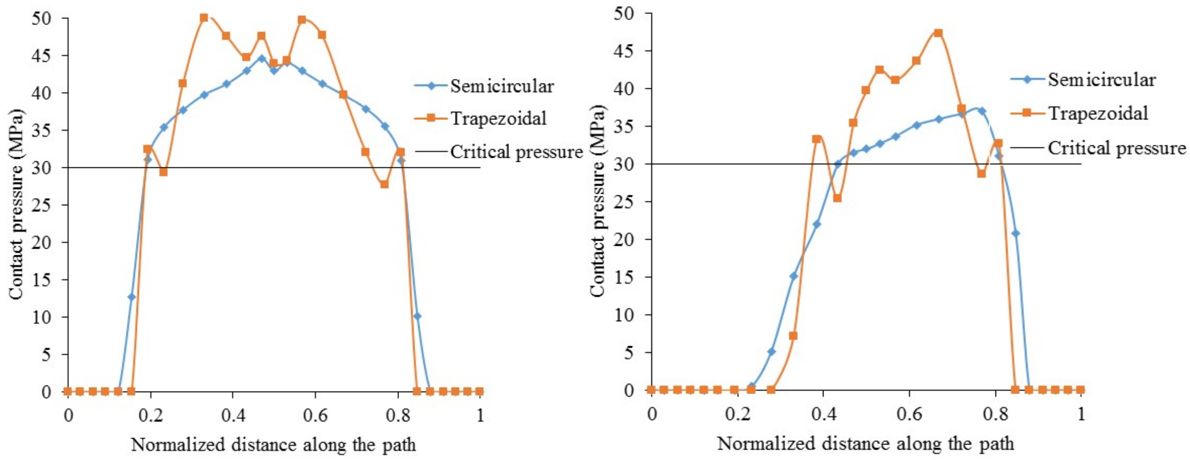

(a) (b)

Fig. 15. Distribution of contact pressure (a) before and (b) after pressure penetration at 0.3 mm interference.

5. Conclusion

A global and a local model of a flexible-pipe end-fitting seal system were developed by FE means. A pressure-penetration module was introduced to these models, and how the contact pressure varied along the leak path under different contact-surface magnitudes of interference and sawtooth shapes was compared and discussed. Using the pressure penetration criterion simulates how the actual working conditions affect the performance of the sealing ring and improves the accuracy to which the performance of the contact seal is evaluated. For the wedge sealing ring, the von Mises stress was larger than any other part of the model, and the results showed that both the contact pressure and contact length increased with the contact magnitude of interference. By comparing the contact pressure and von Mises stress of the sealing structure, the present sealing ring had the best sealing performance when the axial displacement of the sealing ring was 1.2 mm. Introducing the pressure penetration is highly reflective of the working conditions and allows the sealing effectiveness to be checked when the seal structure is subjected to fluid pressure. The results showed that pressure penetration reduced the contact pressure and changed its distribution to a certain extent. In addition, the sawtooth structure of the sealing ring increased the contact pressure along the leak path and improved the sealing capability. To clarify further how the semicircular and trapezoidal sawtooths influence the sealing performance, more-detailed investigation and comparison were conducted. That analysis indicated that the semicircular sawtooth has better sealing performance compared with the trapezoidal sawtooth.

Conflict of Interest

The authors declared no potential conflicts of interest with respect to the research, authorship and publication of this article.

Funding

This research was supported by the China Postdoctoral Science Foundation (grant no. 43XB3793XB), National Key Research and Development Program (grant no. 2018YFC0310204), National Natural Science Foundation of China (grant no. 51674214), and the Scientific Innovation Group for Youths of Sichuan Province (grant no. 2019JDTD0017).

References

[1] Vandyck, T., Kitous, A., Saveyn, B., Keramidas, K., Los Santos, L.R. and Wojtowicz, K., Economic exposure to oil price shocks and the fragility of oil-exporting countries, *Energies*, 11(4), 2018, 827.
[2] Lia, X.T., Vaza, M.A. and Custodiob, A.B., Analytical prediction for lateral buckling of tensile wires in flexible pipes, *Marine Structures*, 61, 2018, 268-281.
[3] Drumond, G.P., Geovana, P., Pasqualino, I.P., Pinheiro, B.C. and Estefen, S.F., Pipelines, risers and umbilicals failures: a literature review, *Ocean Engineering*, 148, 2017, 412-425.
[4] Gadala, I.M., Wahab, M.A. and Alfantazi, A., Electrochemical corrosion finite element analysis and burst pressure prediction of externally corroded underground gas transmission pipelines, *Journal of Pressure Vessel Technology*, 140, 2018, 011701.
[5] Pham, S.C., Sridhar, N., Qian, X., Sobey, A.J. and Achintha, M., A review on design, manufacture and mechanics of composite risers, *Ocean Engineering*, 112, 2016, 82-96.
[6] Li, X., Jiang, X.L. and Hopman. H., A review on predicting critical collapse pressure of flexible risers for ultradeep oil and gas production, *Applied Ocean Research*, 80, 2018, 1-10.
[7] Saevik, S. and Thorsen, M.J., An analytical treatment of buckling and instability of tensile armors in flexible pipes, *Journal of Offshore Mechanics and Arctic Engineering*, 139, 2017, 041701.
[8] Dahl, C.S., Andersen, B. and Groenne, M., Developments in managing flexible risers and pipelines, a supplier's perspective, *Offshore Technology Conference*, Houston, Texas, USA, 2011.
[9] Ebrahimi, A., Kenny, S. and Hussein, A., Radial buckling of tensile armor wires in subsea flexible pipe—numerical assessment of key factors, *Journal of Offshore Mechanics and Arctic Engineering*, 138, 2016, 031701.
[10] Hu, G., Wang, G.R., Dai, L.M., Zhang, P., Li, M. and Fu, Y.K., Sealing failure analysis on V-shaped sealing rings of an inserted sealing tool used for multistage fracturing processes, *Energies*, 11, 2018, 1432.
[11] Zhou, C.L., Zheng, J.Y., Gu, C.H., Zhao, Y.Z. and Liu, P.F., Sealing performance analysis of rubber O-ring in high-pressure gaseous hydrogen based on finite element method, *International Journal of Hydrogen Energy*, 42, 2017, 11996-12004.
[12] Wu, D., Wang, S.P. and Wang, X.J., A novel stress distribution analytical model of O-ring seals under different properties of materials, *Journal of Mechanical Science Technology*, 31, 2017, 289-296.
[13] Wang, L.Q., Wei, Z.L., Yao, S.M., Guan, Y. and Li, S.K., Sealing performance and optimization of a subsea pipeline mechanical connector, *Chinese Journal of Mechanical Engineering*, 31, 2018, 18.
[14] Fernando, U.S., Nott, P., Graham, G., Roberts, A.E. and Sheldrake, T., Experimental evaluation of the metal-to-metal seal design for high-pressure flexible pipes, *Offshore Technology Conference*, Houston, Texas, USA, 2012.
[15] Fernando, U.S. and Karabelas, G., Analysis of end fitting barrier seal performance in high pressure unbonded flexible pipes, *33rd ASME International Conference on Ocean, Offshore and Arctic Engineering*, San Francisco, Canada, 2014.
[16] Li, X.Y., Du, X.Y., Wan, J. and Xiao, H., Structure analysis of flexible pipe end fitting seal system, *Proceedings of the ASME 34th International Conference on Ocean, Offshore and Arctic Engineering*, St. John's, Newfoundland, Canada, 2015.
[17] Zhang, L., Yang, Z.X., Lu, Q.Z., Yan, J., Chen, J.L. and Yue, Q.J., Numerical simulation on the sealing performance of serrated teeth inside the wedgy sealing ring of end ftting of marine fexible pipeline, *Oil & Gas Storage and Transportation*, 37, 2017, 108-115 (in Chinese).
[18] API 17J. *Specification for Unbonded Flexible Pipe*. 4th ed. Washington: American Petroleum Institute, 2014.
[19] API 17B. *Recommended Practice for Flexible Pipe*. 5th ed. Washington: American Petroleum Institute, 2014.
[20] Yan, H., Zhao, Y.L., Liu, J.G. and Jiang, H.Y., Analyses toward factors influencing sealing clearance of a metal rubber seal and derivation of a calculation formula, *Chinese Journal of Aeronautics*, 29, 2016, 292-296.
[21] Yu, R.H. and Yuan, P.B., Structure and research focus of marine unbonded flexible pipes, *Oil & Gas Storage and Transportation*, 35, 2016, 1255-1260 (in Chinese).
[22] Malta, E.R. and Martins, C.D., Finite element analysis of flexible pipes under axial compression: influence of the sample length, *Journal of Offshore Mechanics and Arctic Engineering*, 139, 2017, 011701.
[23] Cuamatzi-Melendez, R., Castillo-Hernandez, O., Vazquez-Hernandez, A.O. and Vaz, M.A., Finite element and theoretical analyses of bisymmetric collapses in flexible risers for deepwaters developments, *Ocean Engineering*, 140, 2017, 195-208.
[24] Hu, G., Wang, G.R., Li, M., He, X. and Wu, W., Study on sealing capacity of packing element in compression

packer, *Journal of the Brazilian Society of Mechanical Sciences and Engineering*, 40, 2018, 438.
[25] Zhao, B., Zhao, Y.J., Wu, X.Y. and Xiong, H.C., Sealing performance analysis of P –shape seal with fluid pressure penetration loading method, *IOP Conference Series: Materials Science and Engineering*, 397, 2018, 012126.
[26] Slee, A.J., Stobbart, J., Gethin, D.T. and Hardy, S.J., Case study on a complex seal design for a high pressure vessel application, *ASME Pressure Vessels and Piping Conference*, Anaheim, California, USA, 2014.
[27] Gorash, Y., Dempster, W., Nicholls, W.D. and Hamilton, R., Fluid pressure penetration for advanced FEA of metal-to-metal seals, *Proceedings in Applied Mathematics and Mechanics*, 15, 2015, 197-198.
[28] Liao, J.J., Smith, D.W., Miramini, S., Thibbotuwawa, N., Gardiner, B.S. and Zhang, L.H., The investigation of fluid flow in cartilage contact gap, *Journal of the Mechanical Behavior of Biomedical Materials*, 95, 2019, 153-164.
[29] *ABAQUS Theory Guide*, Version 2016.

ORCID iD

Liping Tang https://orcid.org/0000-0003-0981-2120
Wei He https://orcid.org/0000-0001-7584-8434
Xiaohua Zhu https://orcid.org/0000-0002-0507-3773
Yunlai Zhou https://orcid.org/0000-0002-2347-647X